Composites: Part A 205 (2026) 109732

Contents lists available at ScienceDirect

Composites Part A

journal homepage: www.elsevier.com/locate/compositesa

Development of self-healing epoxy/COC adhesives for potential use in wind turbine blades

Nicolò Truschelli [a], Laura Simonini [a,b,*], Antonios Tempelis [c], Leon Mishnaevsky Jr. [c], Alessandro Pegoretti [a,b], Andrea Dorigato [a,b]

[a] Department of Industrial Engineering, University of Trento, via Sommarive 9, 38121 Trento, Italy
[b] National Interuniversity Consortium of Materials Science and Technology (INSTM), via Giusti 9, 50121 Florence, Italy
[c] Department of Wind and Energy Systems, Technical University of Denmark, Roskilde 4000, Denmark

HIGHLIGHTS

- EP/COC blends were developed as thermally, self-healable adhesives.
- EP-30 wt% COC repaired at 175 °C achieved fracture toughness recovery of 81 %
- Bonded joints recovered up to 43 % of their lap shear strength.

GRAPHICAL ABSTRACT

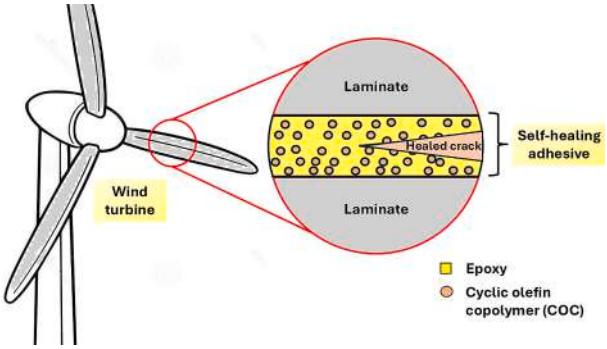

ARTICLE INFO

Keywords:
Epoxy
Adhesive
Self-healing
Wind turbines

ABSTRACT

In this work, epoxy (EP)/cyclic olefin copolymer (COC) blends were investigated as a new type of thermally, self-healable adhesives. Blends, containing 15 and 30 wt% of COC, were formulated, characterized and then applied to epoxy/carbon fiber laminated joints, to evaluate their structural performance and self-healing capabilities. Rheological measurements on uncured blends revealed that storage modulus, loss modulus and complex viscosity of the blends increased with COC content, without compromising the processability of the blends. FTIR and FESEM analyses confirmed the formation of an immiscible morphology of discrete COC domains distributed and weakly bonded to the matrix. Thermal analysis revealed that the adhesives had good thermal stability, while mechanical tests showed a moderate reduction in tensile strength and fracture toughness upon COC introduction, due to the limited EP/COC interfacial adhesion. During the self-healing process at 175 °C, the COC phase softened and flowed into the damaged area and the blend containing 30 wt% of COC achieved a recovery in fracture toughness (K_{IC}) of 81 %. In the bonded joints, the application of the adhesive with 30 wt% of COC allowed to recover about 43 % of the original lap shear strength. This adhesive effectively achieved a balance between mechanical performance and self-healing capability.

* Corresponding author at: Department of Industrial Engineering, University of Trento, via Sommarive 9, 38121 Trento, Italy.
E-mail address: laura.simonini@unitn.it (L. Simonini).

https://doi.org/10.1016/j.compositesa.2026.109732
Received 3 December 2025; Received in revised form 23 February 2026; Accepted 10 March 2026
Available online 11 March 2026
1359-835X/© 2026 The Authors. Published by Elsevier Ltd. This is an open access article under the CC BY-NC-ND license (http://creativecommons.org/licenses/by-nc-nd/4.0/).

1. Introduction

Wind energy is one of the most promising renewable energy sources and it plays key role in the transition towards a sustainable power generation. According to the Global Wind Energy Council (GWEC), the installed wind capacity has surpassed 1136 GW in 2024, with an increasing portion coming from offshore systems [1]. Compared to onshore systems, offshore wind farms benefit from stronger and more consistent wind conditions, therefore they enable a large-scale energy production [2–4]. However, they operate in harsh environments, where the maintenance and the repairing operations are technically complex and expensive. Wind turbines are composed of three main parts: (i) the rotor, which consists of blades and hub; (ii) the nacelle, which houses the gearbox, generator and control systems; (iii) the tower, which supports this assembly and transfers the loads to the foundation [5]. The blades are the most critical and expensive components, as they must combine lightweight with high stiffness and strength. They are usually made of two skins of fiber-reinforced polymer (FRP) composite, separated by internal spar caps and shear webs [6,7]. The skins and the internal components are bonded together by adhesives, typically based on epoxy resins (EP). The huge size of the modern offshore blades, which may exceed 100 m in length, subjects the adhesives to high loads. The consequence is that even minor defects within these adhesives can result in critical damage and failure of the blade [7–11]. Therefore, to guarantee the structural integrity of wind turbines throughout their operational lifespan, it is essential to improve the performance and durability of the adhesives.

One promising approach is the development of self-healing adhesives, that can autonomously repair microcracks and restore the mechanical integrity after a damage [12]. Self-healing materials can be classified in: (i) intrinsic systems, which enable multiple self-healing events via reversible chemical bonds or the introduction of a thermoplastic phase [13–19] and (ii) extrinsic systems, which enable a single self-healing event by releasing the encapsulated healing agent into the cracks [20–22]. Despite their potential, most self-healing systems are mechanically inadequate for structural applications due to their inherently weak mechanical properties. For example, intrinsic systems such as Diels–Alder based epoxies or supramolecular polymers can achieve excellent healing efficiencies but typically suffer from reduced stiffness and load-bearing capacity because the reversible bonds weaken the overall rigidity of the network [23]. Strachota et al. showed that Diels–Alder/epoxy networks achieved nearly 100 % self-healing, but the system exhibited limited mechanical properties [24]. On the other hand, the solid microcapsules in extrinsic systems act as stress concentrators within the matrix, thereby reducing the material's stiffness and overall mechanical strength [25]. For example, Malekkhouyan et al. demonstrated that while the incorporation of microcapsules into self-healing polymers coatings enhanced the healing performance of the matrix, it significantly weakened the overall mechanical properties due to the reduced capsule/matrix interfacial adhesion [26]. Therefore, it is crucial to develop structural adhesives for wind turbine blades that offer both high mechanical performance and self-healing efficiency in a single, load-bearing material.

In this scenario, cyclic olefin copolymers (COCs) are particularly promising as self-healing agents in epoxy-based systems [27]. COC is a thermoplastic polymer characterized by a relatively high glass transition temperature (about 70 °C), excellent thermal stability and good mechanical strength, which make it compatible with structural applications [28]. Unlike many soft thermoplastics or reversible chemistries approaches commonly used in intrinsic self-healing materials, at room temperature COC exhibits mechanical properties comparable to those of epoxy resins. Its elastic modulus ranges from 1.8 to 2.6 GPa and its tensile strength from 50 to 70 MPa [29], while epoxy typically shows an elastic modulus from 2.5 to 3.5 GPa and a tensile strength from 60 to 90 MPa [30]. This similarity ensures that the incorporation of COC does not significantly compromise the stiffness or strength of the epoxy matrix, making it particularly suitable for structural self-healing applications. In previous works of our group [31,32], blends of EP containing from 10 up to 40 wt% of COC were systematically investigated and optimized for self-healing applications. These works demonstrated that the immiscible COC phase in EP did not substantially alter the load-bearing capacity of the resulting materials. Furthermore, COC softened and partially flowed upon heating above 170 °C, allowing the closure of microcracks and the recovery of up to 90 % of the original fracture toughness (K_{IC}). These promising results suggested that EP/COC blends could be used in structural self-healing systems, and they could be thus employed in the development of self-repair adhesives for composite structures, such as wind turbine blades.

Therefore, this work explored EP/COC blends as a new type of thermally self-healable adhesives. To the best of the authors' knowledge, no previous study has reported the development and characterization of such structural adhesives. The work was divided into two main parts: (i) the formulation and characterization of EP/COC adhesive blends, and (ii) the fabrication and testing of bonded joints. The adhesive blends were characterized in terms of their microstructural, thermal, and mechanical properties. Self-healing was thermally activated at temperatures of 145 °C and 175 °C and the self-healing efficiency was evaluated based on the recovery of their fracture toughness. Then, the adhesive blends were used to fabricate bonded joints, whose self-healing efficiency was assessed at 175 °C in terms of recovery of their lap shear strength.

2. Experimental part

2.1. Materials

For the preparation of the adhesive blends, epoxy resin (EP) was used as the thermoset matrix. It was provided by Elantas Europe S.r.l. (Colecchio, Italy) and it was composed of an epoxy base (Elan-tech AS 90, density = 1.18 g/cm^3, viscosity = 400 Pa•s at 25 °C) and hardener (Elan-tech AW 90, density = 0.98 g/cm^3, viscosity = 125 Pa•s at 25 °C) mixed at a weight ratio 100:45. A curing cycle of 2.5 h at room temperature and 5 h at 70 °C was recommended by the producer. As reported in the datasheet, the cured system had a density of 1.08–1.12 g/cm^3 and a glass transition temperature (T_g) of 70–75 °C. Cyclic olefin copolymer (COC) (Topas 8007S-04) was used as the healing agent. It was provided by Topas Advanced Polymers GmbH (Raunheim, Germany) in form of granules of 3 mm, it was constituted by 65 wt% of norbornene and 35 wt% of ethylene. As reported in the datasheet, it had density of 1.01 g/cm^3, a Melt Flow Index (MFI) of 1.7 g/10 min (190 °C, 2.16 kg) and glass transition temperature of 78 °C.

For the preparation of the bonded joints, a different epoxy system was used as the thermoset matrix. It was provided by Elantas Europe S.r.l. (Colecchio, Italy) and it consisted of an epoxy a base (Elan-tech EC 157, density = 1.15 g/cm^3, viscosity = 0.7 Pa•s at 25 °C) and an hardener (Elan-tech W 324, density = 0.95 g/cm^3, viscosity = 0.05 Pa•s at 25 °C) mixed at weight ratio 100:30. A curing cycle of 24 h at room temperature and 16 h at 60 °C was recommended by the producer. As reported in the datasheet, the cured system had density of 1.10 g/cm^3 and glass transition temperature of 88–92 °C. Carbon fibers (CFs) (GV-201 U TFX) were used as the reinforcing phase. They were provided by Cristex Composite Materials LDT (Blackburn, UK) in the form of a unidirectional fabric, having a nominal surface density of 218 g/m^2 ±5 % and an average fiber diameter of 8 μm.

2.2. Sample preparation

2.2.1. Preparation of the adhesive blends

Before processing, COC granules were cryo-grinded by using an Ika Werke M20 grinder (Ika AG, Staufer, Germany) and sieved to obtain particles smaller than 300 μm, and then dried in an oven at 50 °C for 12 h. Subsequently, epoxy base (AS 90) and hardener (AW 90) were

weighed into separate beakers, then heated at 50 °C for 20 min to decrease their viscosity. The required amount of COC was weighed and distributed equally between the two beakers and manually mixed for 2 min. Once the mixtures were homogeneous, they were combined and manually mixed at 50 °C for 2 min, and then poured into silicon molds, having dimensions corresponding to 1BA specimens for tensile tests (ISO 527) and 44 x 10 x 5 mm^3 for specimens for fracture toughness tests. The resulting materials were cured at room temperature for 2.5 h and then in an oven at 70 °C for 5 h. The list of the prepared samples, with their relative composition, is summarized in Table 1.

2.2.2. Preparation of the bonded joints

Joints were composed of two adherends bonded together by the adhesive, as schematically depicted in Fig. 1. The adherends were prepared by using a combination of hand lay-up and vacuum bagging techniques. First, ten carbon fiber laminae of 22 × 22 mm^2 were laid on a flat metal plate and manually impregnated with the epoxy base (EC 157)/hardener (W 342) liquid mixture. The entire assembly was sealed using a vacuum bag on the metal plate with sealant tape and vacuum was applied to ensure proper compaction and resin distribution. The composite structure was cured at room temperature for 24 h, demolded and post-cured at 60 °C for 15 h. Then, adherends were cut from the prepared laminates in rectangular pieces having dimensions 101.6 x 25.4 x 3.6 mm^2.

Hence, the joints were prepared by placing the uncured EP/COC blend adhesives between two adherends to cover an overlapping area of 25.4 × 12.5 mm^2. The thickness of the adhesive layer was fixed at 0.75 mm by placing two copper wires at the boundaries of the adhesive area. This procedure has been already used by our research group in previous studies on the adhesive properties of composite joints, as it guaranteed a homogeneous adhesives thickness [33,34]. However, it is well known that the insertion of these copper wires could slightly alter the stress distribution at the joint ends, affecting the overall mechanical performance of the junction [35]. In the future investigations some efforts will be required to improve the junction design, and less invasive techniques to obtain a uniform adhesive layer within the overlapping area will be considered. The joints were then cured under the same conditions adopted for the EP/COC blends (i.e. 2.5 h at room temperature, then 5 h at 70 °C) under a weight of 1 kg. Joint samples were designated by adding "j" at the beginning of the corresponding adhesive name (i.e. j_EP-15 represents a joint bonded by using the adhesive EP-15).

2.3. Experimental techniques

2.3.1. Characterization of the EP/COC adhesive blends

The dynamic rheological properties of the uncured blends were analyzed using a Discovery Hybrid Rheometer (DHR-2) (TA Instruments Inc., New Castle, DE, USA) by adopting a plate–plate configuration, with a plate diameter of 25 mm and distance gap of 1 mm. Tests were carried out at 70 °C, to simulate the material processability at the curing temperature, by applying a strain amplitude of 1 %. In this way, the trends of the storage modulus (G'), loss modulus (G'') and complex viscosity (η^*) were investigated in an angular frequency (ω) range between 0.1 and 100 rad/s. One specimen was tested for each composition.

The chemical properties of the blends were analyzed by using Fourier transform infrared spectroscopy (FTIR) in attenuated total reflectance mode using a Perkin Elmer Spectrum One FTIR spectrometer (Perkin Elmer Inc., Shelton, CT, USA). Four scans between 4000 and 650 cm^{-1} were performed for each sample, with a 4 cm^{-1} resolution. One specimen was tested for each composition.

Table 1
List of the prepared samples.

Samples	Base AS 90 (wt%)	Hardener AW 90 (wt%)	COC (wt%)
EP	69.0	31.0	–
EP-15	58.6	26.4	15.0
EP-30	48.3	21.7	30.0

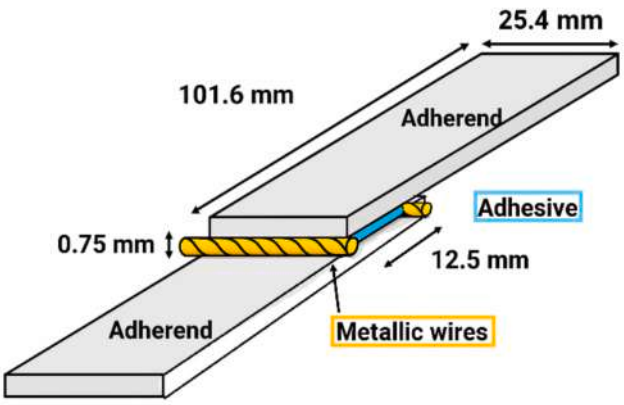

Fig. 1. Schematic representation of an epoxy/CF bonded joint.

The morphological features of the blends were observed on the cryo-fractured and healed surfaces of the samples by using a field emission scanning electron microscope (FESEM). The analysis was conducted by using a Zeiss Supra 40 microscope (Carl Zeiss AG, Oberkochen, Germany) operating at an accelerating voltage of 3.5 kV. Prior to FESEM analysis, the samples were coated with a layer of a platinum/palladium (Pt/Pd) alloy (80:20) with a thickness of about 5 nm. The void volume fraction (V_v) of the blends was calculated as reported in Eq. (1):

$$Vv = \frac{\rho_{th} - \rho_{exp}}{\rho_{th}} \quad (1)$$

where ρ_{exp} is the experimental density of the blends measured by an Accupyc 1330 helium pycnometer (Micromeritics Instrument Corporation, Norcross, GA, USA), and ρ_{th} is the theoretical density calculated as reported in Eq. (2):

$$\rho_{th} = \frac{1}{\sum_i \frac{w_i}{\rho_{i,exp}}} \quad (2)$$

where w_i and $\rho_{i,exp}$ are the weight fraction and the experimental density of each constituent in the blends. At least three specimens were tested for each composition.

Differential scanning calorimetry (DSC) tests were conducted on the blends through a Mettler DSC 5+ calorimeter (Mettler Toledo Inc., Columbus, OH, USA) under a nitrogen flow of 100 mL/min, in a temperature range from 0 °C to 200 °C, at a heating/cooling rate of 10 °C/min. All blends were subjected to a first heating scan, a cooling scan, and a second heating scan. In this way, the glass transition temperature of the EP ($T_{g,EP}$) and of the COC ($T_{g,COC}$) were analyzed. One specimen was tested per composition. Thermogravimetric analysis (TGA) of the blends was carried out using a Mettler TG50 thermobalance (Mettler Toledo Inc., Columbus, OH, USA) under a nitrogen flow of 100 mL/min in a temperature interval from 30 to 700 °C at a heating rate of 10 °C/min. The tests allowed to measure the temperature associated with a mass loss of 1 wt% ($T_{1\ \%}$) and the maximum degradation temperature (T_d) of EP and COC, which corresponds to the peak of the derivative thermogravimetric curve (DTG). Moreover, the residual mass after the test (m_{700}) was taken. One specimen was tested per composition. The thermal diffusivity (α), the specific heat capacity (c_p) and the thermal conductivity (λ) of the blends were measured at 20 °C using laser flash analysis (LFA) with a Netzsch LFA 447 instrument (Netzsch Gerätebau GmbH, Selb, Germany). Three circular specimens with a diameter of 12.7 mm and a thickness of 2 mm were tested for each composition.

Quasi-static tensile properties of the blends at room temperature

were analyzed using an Instron® 5969 universal testing machine (Instron Inc., Norwood, MA, USA) equipped with a load cell of 10 kN. 1BA-type dumbbell specimens, having a gage length of 25 mm, were tested according to the ISO 527 standard. The elastic modulus (E) was measured at a crosshead speed of 0.25 mm/min, imposing a maximum axial deformation level of 1 %. The strain was recorded using a dynamic extensometer Instron® model 2620–601 (gauge length of 12.5 mm) and, according to the ISO 527 standard, the elastic modulus was determined as a secant value between deformation levels of 0.05 % and 0.25 %. Tensile properties at break were evaluated at a crosshead speed of 1 mm/min, without using the extensometer. The stress at break (σ_b) and the elongation at break (ϵ_b) were determined. At least five specimens were tested for each formulation.

The fracture toughness of the blends was evaluated according to ASTM D5045 standard. The tests were carried out on Single Edge Notched Bending (SENB) specimens, having nominal dimensions of 44 x 10 x 5 mm^3, an initial notch length of 5 mm and a span length of 40 mm. At least 5 specimens were tested for each composition. Tests in quasi-static mode were performed in three-point bending configuration by using an Instron® 5969 universal testing machine with a crosshead speed of 10 mm/min. From the load–displacement curves it was possible to determine the maximum load (P_{max}) sustained by the samples. From this value, the critical stress intensity factor (K_{IC}) was calculated according to Eq. (3):

$$K_{IC} = \frac{P_{max}}{B\sqrt{W}} \bullet f(x) \tag{3}$$

where f(x) is a finite value expressed in the standard as a function of x = a/W, B and W represent the thickness and width of the specimens, respectively, while a is the notch length. Furthermore, accordingly to ASTM D5045 standard, from the integration of the load–displacement curves and the evaluation of system compliance, also the critical strain energy release rate (G_{IC}) values in quasi-static mode were obtained, according to the expression reported in Eq. (4):

$$G_{IC} = \frac{\Delta U}{BW\varphi} \tag{4}$$

where ΔU is the difference of the total energy absorbed by the sample and the energy absorbed in the indentation tests, and φ is a finite value and provided in the standard as function of x = a/W.

2.3.2. Characterization of the bonded joints

The lap shear tests were conducted on the joints according to ASTM D5868 standard. The tests were carried out at room temperature under quasi-static conditions by using Instron® 5969 universal testing machine (Instron Inc., Norwood, MA, USA) equipped with a load cell of 50 kN. The maximum shear load withstand by the joints (P_{max}) was measured at crosshead speed of 13 mm/min on at least five specimens for each composition. Therefore, the maximum shear strength (τ_{max}) was calculated as reported in Eq. (5), where A is the overlapping area :

$$\tau_{max} = \frac{P_{max}}{A} \tag{5}$$

2.3.3. Evaluation of the self-healing efficiency

After being tested, the broken SENB specimens were placed in an iron vice under a pressure of 0.5 MPa and heated in an oven at 145 °C or 175 °C for 60 min. Then, the healed samples were tested again in quasi-static mode in order to calculate the fracture toughness ($K_{IC,H}$) and the critical strain energy release rate ($G_{IC,H}$) of the healed samples The self-healing efficiency ($HE_{K_{IC}}$ and $HE_{G_{IC}}$) was calculated by using the expressions reported in Eqs. (6) and (7):

$$HE_{K_{IC}} = \frac{K_{IC,H}}{K_{IC}} \tag{6}$$

$$HE_{G_{IC}} = \frac{G_{IC,H}}{G_{IC}} \tag{7}$$

Similarly, the broken joint specimens were placed in an iron vice under a pressure of 0.5 MPa and heated in an oven at 175 °C for 60 min. Then, the healed samples were tested again in lap shear mode and the shear strength of the healed samples ($\tau_{max,H}$) was obtained. The healing efficiency (HE_τ) was evaluated by using the expression reported in Eq. (8):

$$HE_\tau = \frac{\tau_{max,H}}{\tau_{max}} \tag{8}$$

The morphological features of the overlapping area in the broken and in the healed joins were evaluated by using a Nikon SMZ25 (Nikon Corporation, Tokyo, Japan) optical microscope (OM).

3. Results and discussion

3.1. Characterization of the adhesive blends

3.1.1. Rheological measurements

In Fig. 2(a-c), the results obtained from the dynamic rheological measurements on the uncured EP/COC blends at 70 °C in terms of storage modulus (G′), loss modulus (G″), and complex viscosity (η*) are respectively reported.

As shown in Fig. 2a, G′ increases with the addition of COC across the entire frequency range, suggesting that the macromolecular mobility of EP is restricted by the presence of the dispersed COC domains. The G″ follows a similar trend, increasing as a function of angular frequency and COC amount (Fig. 2b). This indicates an enhanced viscous dissipation, which is consistent with the coexistence of two immiscible polymeric phases that exhibit partial interfacial compatibility [36]. However, G′ is consistently higher than G″ for all the compositions across the entire investigated frequency range, confirming the predominance of the elastic component in the rheological behaviour of these blends. The complex viscosity (Fig. 2c) shows the typical shear-thinning trend characteristic of polymeric materials, where viscosity decreases with increasing angular frequency. Moreover, the viscosity slightly increases with COC loading, reflecting a reduced chain mobility and a partial interfacial interaction between EP and COC [36]. However, this increase is not dramatic, so that the processability of the material is not compromized [37]. Furthermore, Fig. 2d illustrates the complex viscosity of COC at healing temperatures of 145 °C and 175 °C. The rheological trends demonstrate that temperature fundamentally affects the viscosity of COC, indeed, the higher the temperature, the lower the viscosity, especially in the low shear rate region. These results confirm the importance of temperature in activating the healing mechanism, since the healing agent must be able to flow properly into the fracture surface and fill the crack.

3.1.2. Microstructural characterization

In Fig. 3(a,b) the FTIR spectra on the prepared blends are shown.

The FTIR spectrum of EP exhibits the characteristic absorption bands of a crosslinked epoxy network [38], i.e., the broad O—H stretching at approximately 3300 cm^{-1}, the C—H stretching between 3000 and 2850 cm^{-1}, the C≡N stretching at approximately 2250 cm^{-1} and the C═C stretching at around 1600 cm^{-1}. Moreover, the peak observed between 1450 and 1370 cm^{-1} correspond to CH_2 and CH_3 bending, respectively, while the strong bands between 1250 and 1100 cm^{-1} are assigned to C—O—C stretching vibrations, which are typical of the chemical bonds formed after epoxy ring opening. The COC spectrum shows distinct CH_2 and CH_3 stretching modes and lacks the O—H vibration. The spectra of the EP/COC blends (EP-15 and EP-30) show a combination of the characteristic peaks of the two components without the appearance of new bands. This observation confirms the absence of strong chemical interactions between EP and COC. However, the slight variation in the

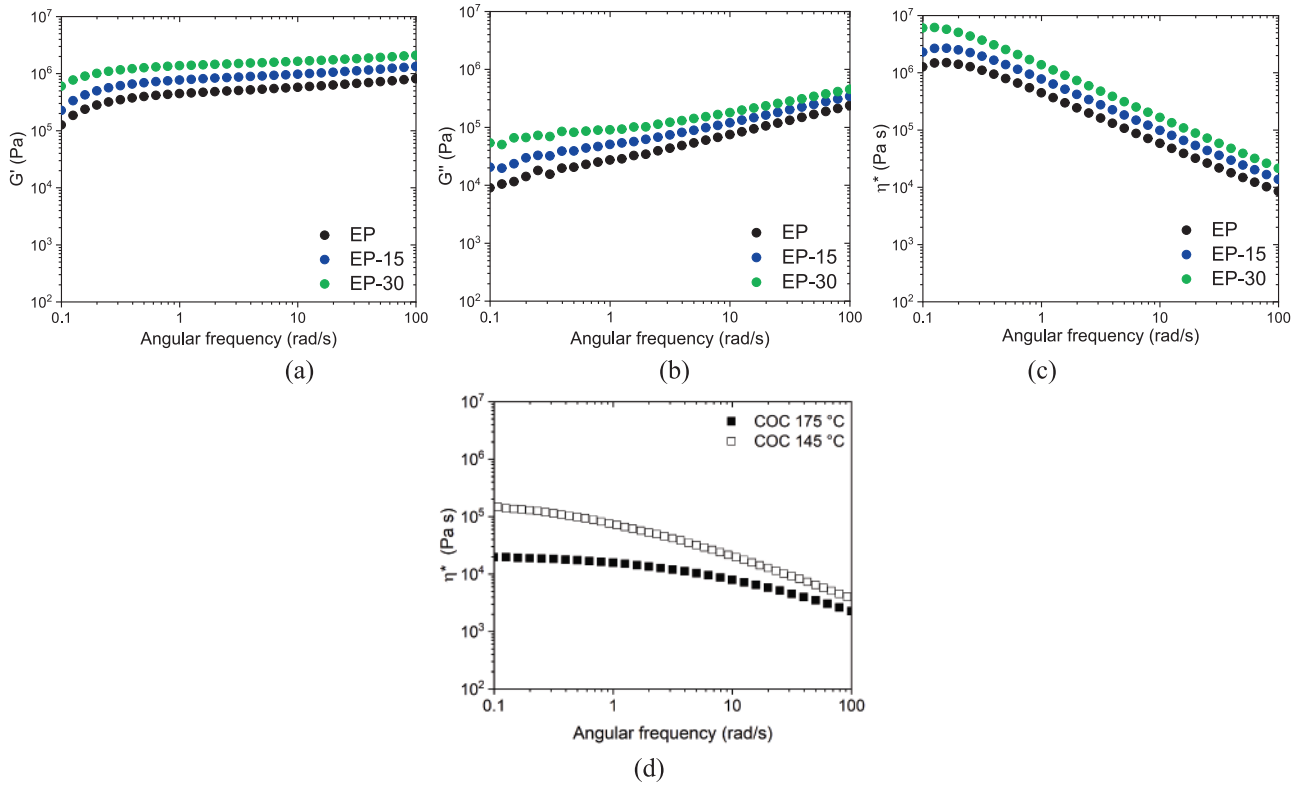

Fig. 2. Dynamic rheological properties of the EP/COC adhesives as a function of angular frequency: (a) storage modulus, (b) loss modulus and (c) complex viscosity measured at 70 °C before curing. (d) Dynamic rheological properties of COC: complex viscosity values measured at 145 °C and 175 °C.

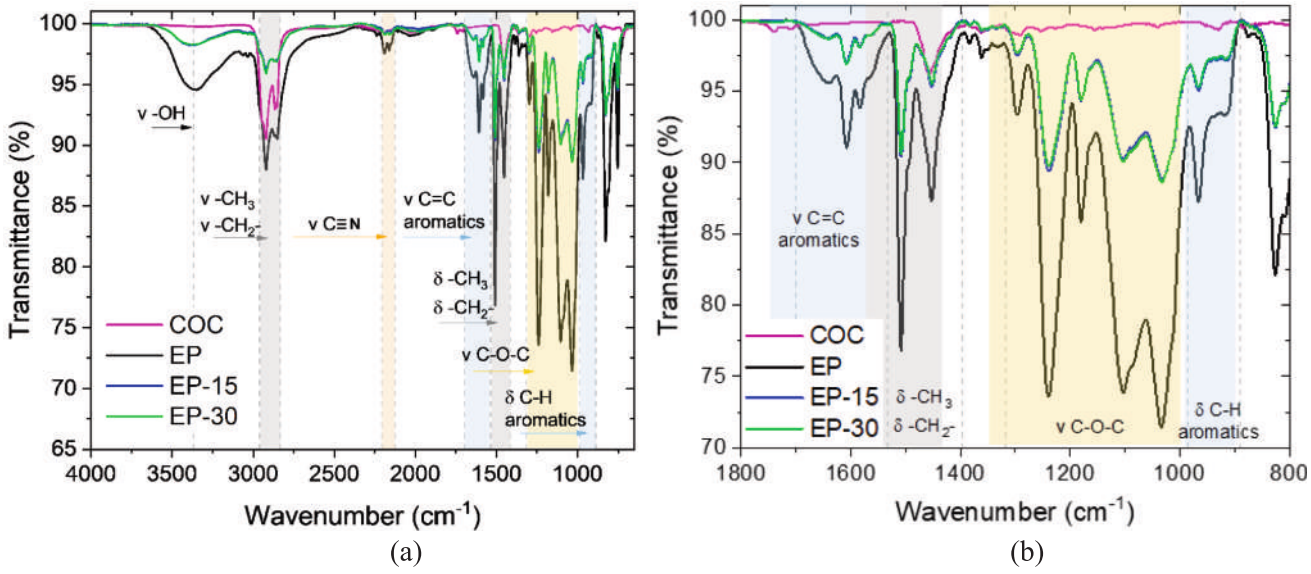

Fig. 3. FTIR spectra of the prepared blends: (a) from 4000 to 650 cm^{-1} and (b) zoom from 1800 to 800 cm^{-1}.

position of the O—H band observed with COC introduction (approximately 3380 cm^{-1}) can be attributed to weak intermolecular interactions, such as hydrogen bonds, acting at the interface between the two phases [39].

Fig. 4(a-d) shows the FESEM micrographs of the COC particles and the prepared EP/COC blends.

After cryo-grinding and sieving, the COC particles appear irregularly shaped, with an average size of 125 ± 61 μm (see Fig. S1 in the Supplementary Materials). The fracture surface of the EP matrix exhibits a relatively rough morphology with some voids. In EP-15 and EP-30, the COC domains are randomly dispersed as discrete particles within the EP phase, with limited agglomeration. The particles demonstrate limited interfacial adhesion with the surrounding matrix, as evidenced by the formation of small interfacial micro-voids and debonded areas around the COC phase. The void volume fractions of blends are summarized in Table 2, along with theoretical and experimental densities of the blends.

The void volume fractions of EP/COC blends are estimated to be 0.1 %, 4.6 % and 2.2 % for EP, EP-15 and EP-30, respectively. The higher void content of EP-15 and EP-30 compared to EP may be due to their higher viscosity during processing.

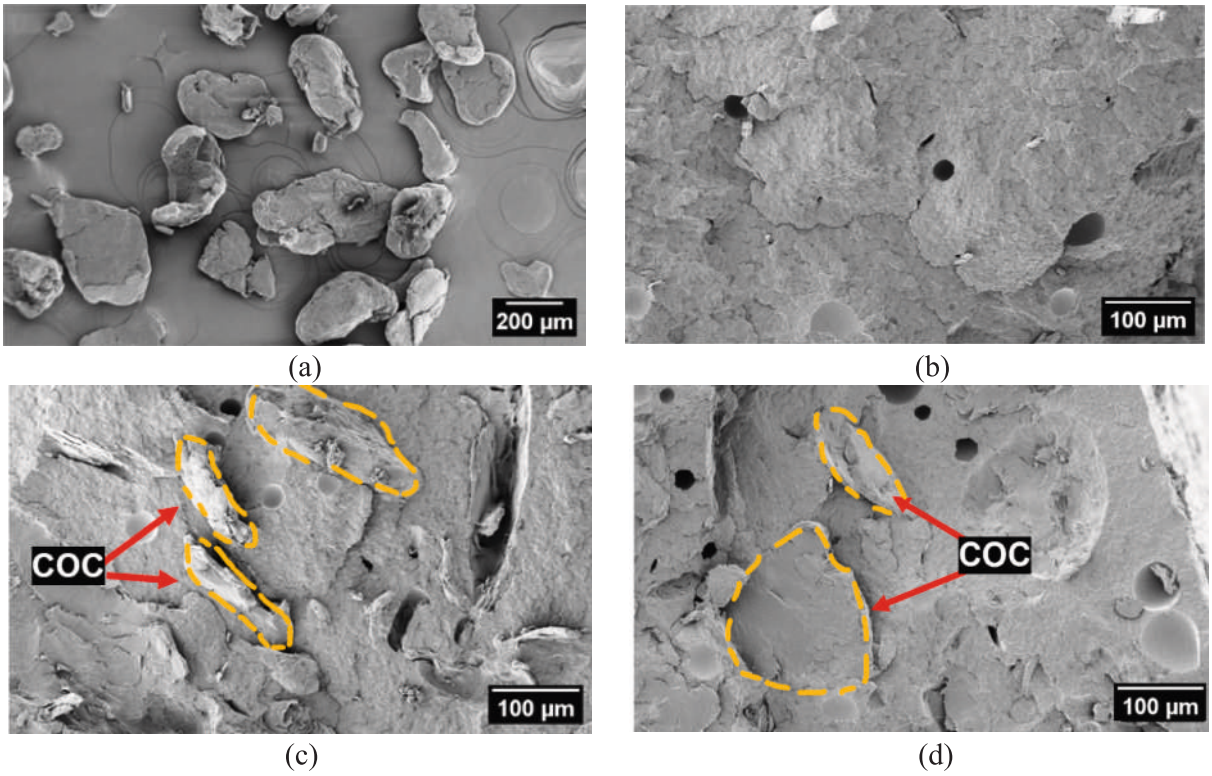

Fig. 4. FESEM micrographs of (a) COC particles, (b) neat epoxy (EP), (c) EP-15, (d) EP-30 blends.

Table 2
Experimental density, theoretical density and voids volume fraction of EP/COC blends.

	ρ_{exp} (g/cm^3)	ρ_{th} (g/cm^3)	V_v (%)
EP	1.099 ± 0.003	1.100 ± 0.020	0.1 ± 0.1
EP-15	1.030 ± 0.002	1.080 ± 0.003	4.6 ± 0.1
EP-30	1.038 ± 0.002	1.061 ± 0.004	2.2 ± 0.2

3.1.3. Thermal characterization

The DSC thermograms revealed no significant differences in the thermal properties of the EP after the incorporation of COC. Therefore, these results are reported in the Supplementary Material (Fig. S2 and Table S1). The glass transition temperatures (T_g) of EP and COC are very close, making them difficult to distinguish. The lack of endothermic peaks in the first and second heating scans, together with the limited increase in the T_g of the EP in the second scan, indicate that a complete curing was achieved in the blends.

Fig. 5(a,b) shows the TGA thermograms and the derivative thermogravimetric (DTG) curves of the prepared blends, while the most important results are summarized in Table 3.

The COC particles undergo a single-step degradation, starting at 435 °C and reaching the maximum degradation rate at temperatures above 480 °C. Furthermore, they undergo complete thermal degradation, leaving no residual mass at 700 °C. In contrast, EP loses 1 % of its

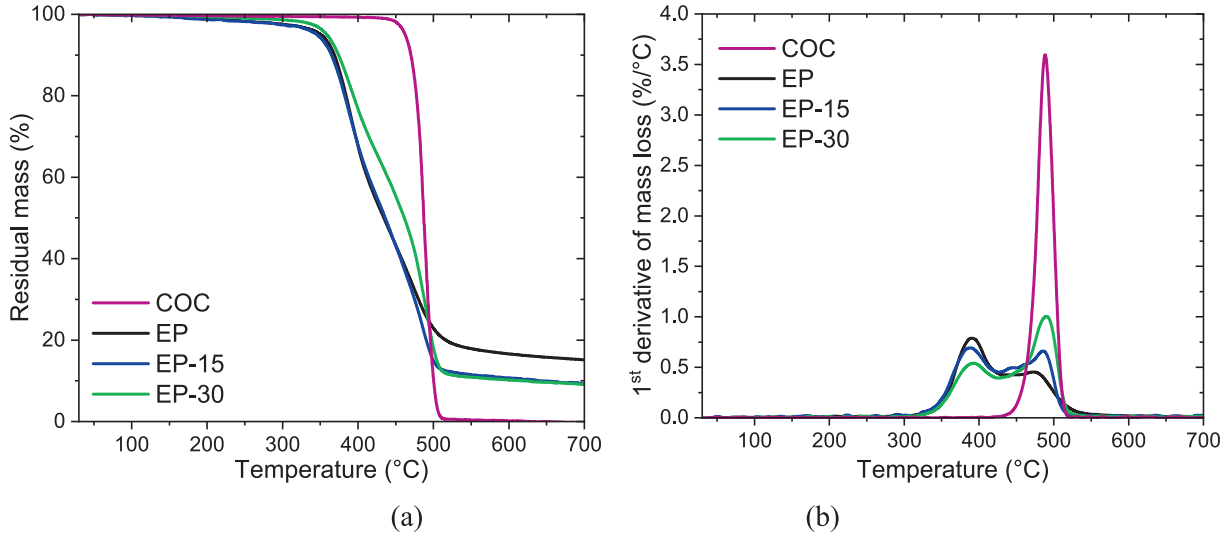

Fig. 5. TGA tests on the prepared EP/COC blends. Trends of (a) residual mass and (b) mass loss derivative as a function of temperature.

Table 3
Results of the TGA analysis performed and the prepared EP/COC blends.

Samples	$T_{1\ \%}$ (°C)	$T_{d,EP}$ (°C)	$T_{d,COC}$ (°C)	m_{700} (%)
EP	198.3	390.5	–	15.2
EP-15	248.3	388.7	485.4	9.7
EP-30	256.2	392.3	490.0	9.2
COC	434.7	–	488.5	0.0

mass at about 200 °C, reaching the maximum degradation rate below 400 °C. The residual mass at the end of the thermal treatment is 15.2 %, which is a typical value for epoxy-based materials [40]. The EP-15 and EP-30 blends exhibit an intermediate thermal behaviour, with a two-step degradation process related to the presence of both the epoxy and the COC phases. They start to degrade at around 250 °C, reaching the maximum degradation rates at about 390 °C(EP phase) and 490 °C (COC). A residual mass of around 9–10 % remains at the end of the thermal test, which is lower than that of the EP sample. This is due to the partial replacement of EP by COC. Overall, the blends exhibit higher thermal stability compared to neat EP, therefore the introduction of COC could be beneficial to the improvement of the blends' resistance to thermal degradation.

The LFA analysis revealed no significant variations in the thermal properties of the EP phase after the incorporation of COC. Therefore, these results are reported in the Supplementary Material (see Fig. S3). The values of thermal diffusivity (α), specific heat capacity (c_p) and thermal conductivity (λ) remain within the range of experimental variation for all compositions. This suggests that the addition of COC does not significantly impact the heat transfer properties of the epoxy matrix. This conclusion will be very important for the modelling of the thermally activated self-healing of these materials.

3.1.4. Mechanical characterization

Fig. 6 shows the representative stress–strain curves from the tensile tests performed on the prepared blends, while Table 4 summarizes the main results.

The stress–strain curves from quasi-static tensile tests show that all samples exhibit a linear elastic region, followed by a strain softening and subsequent failure. The incorporation of COC slightly increases the elastic modulus, from 1.65 GPa to 1.75 GPa at a COC content of 30 wt%, indicating a moderate stiffening effect. However, a reduction in tensile strength and elongation at break is observed as the content of COC

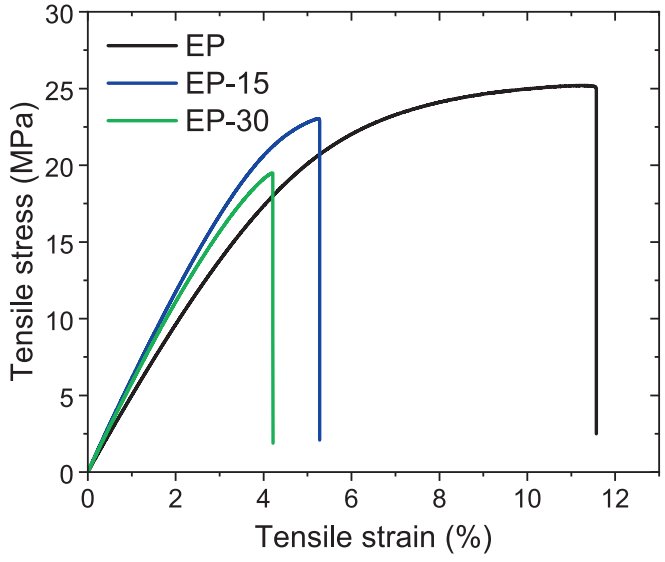

Fig. 6. Representative stress–strain curves from quasi-static tensile tests on the prepared blends.

Table 4
Results of quasi-static tensile tests on the prepared blends.

Samples	E (GPa)	Σ_b (MPa)	E_b (%)
EP	1.65 ± 0.29	30.2 ± 1.3	13.0 ± 1.3
EP-15	1.73 ± 0.15	24.0 ± 0.8	5.4 ± 0.6
EP-30	1.75 ± 0.24	20.5 ± 0.8	4.2 ± 0.3

increases. Indeed, at a COC concentration of 30 wt%, the tensile strength is reduced by 40 %, and the elongation at break by 70 %, compared to neat epoxy. This behaviour suggests that there is a limited interfacial adhesion between the EP and the COC, which could be improved in a future development of this work by using a proper compatibilizing agent.

3.1.5. Fracture behaviour and evaluation of the self-healing efficiency

Fig. 7(a-d) shows the representative load–deflection curves from fracture tests performed on the SENB samples, while Table 5 summarizes the main results.

As can be observed from the curves in Fig. 7a, EP exhibits the highest load-bearing capacity, while the two blends have lower maximum loads and reduced fracture toughness. Indeed, both the K_{IC} and G_{IC} decrease with the addition of COC. For instance, for the EP-30 sample a reduction in K_{IC} and G_{IC} of 26 % and 23 % is respectively registered. Interestingly, the EP-30 sample shows slightly higher K_{IC} and G_{IC} values than EP-15. This could be attributed to the formation of micro-voids through cavitation or particle debonding at higher COC loading. A similar phenomenon was previously observed by Perin et al. [36], who explained that the stress state of the surrounding matrix can change during particle debonding, enabling the matrix to yield and to undergo a plastic deformation. The FESEM micrographs, reported in Fig. 8(a-c), further corroborate these findings. They were taken after quasi-static flexural tests on SENB specimens of EP, EP-15 and EP-30. The micrographs confirm the presence of dispersed COC domains within the epoxy matrix. The domains appear to be weakly bonded to the matrix, as cavities and micro-voids are visible at the EP/COC interface. Therefore, COC acts as stress concentrator and initiator of debonding phenomena, which lead to a localised plasticity of the matrix and to an increase in the fracture toughness behaviour, particularly at higher COC content. Consequently, although the presence of COC reduces the overall fracture toughness of the system, the associated plasticization effect helps to partially mitigate this reduction. Considering the potential application of these blends as structural adhesives, it can be concluded that they exhibit suitable fracture toughness values, in agreement with the values reported in the literature [31,32].

The load–deflection curves of the EP/COC after thermal healing are shown in Fig. 7(b-d). Regardless of the applied temperature, the EP sample shows no toughness recovery, confirming the absence of any intrinsic self-healing mechanism. By contrast, the EP/COC blends exhibit partial recovery of the load-bearing capacity, which is more pronounced at 175 °C due to the lower viscosity of COC, which allows it to flow more easily into the damaged areas (see Fig. 2d). Indeed, the COC domains appear to be adherend to the epoxy matrix, forming a film of molten polymer that partially covers the damaged areas (Fig. 8(h,i)). The K_{IC} and G_{IC} of the healed blends increase significantly with both COC content and healing temperature. For example, when 15 wt% of COC is added in the epoxy matrix, a self-healing efficiency .$HE_{K_{IC}}$ of 20 % at 145 °C and 52 % at 175 °C is obtained, while at 30 wt% of COC a $HE_{K_{IC}}$ of 23 % at 145 °C and of 81 % at 175 °C can be achieved. A similar trend is observed for $HE_{G_{IC}}$, where the sample ^{175}EP-30 reaches the highest self-healing efficiency values (i..e, 55 %). Notably, the quadratic proportionality condition between K_{IC} and G_{IC} was verified for all specimens. Overall, these results demonstrate that the COC phase is essential for self-healing and a temperature of about 175 °C is required to substantially enhance the repair capability.

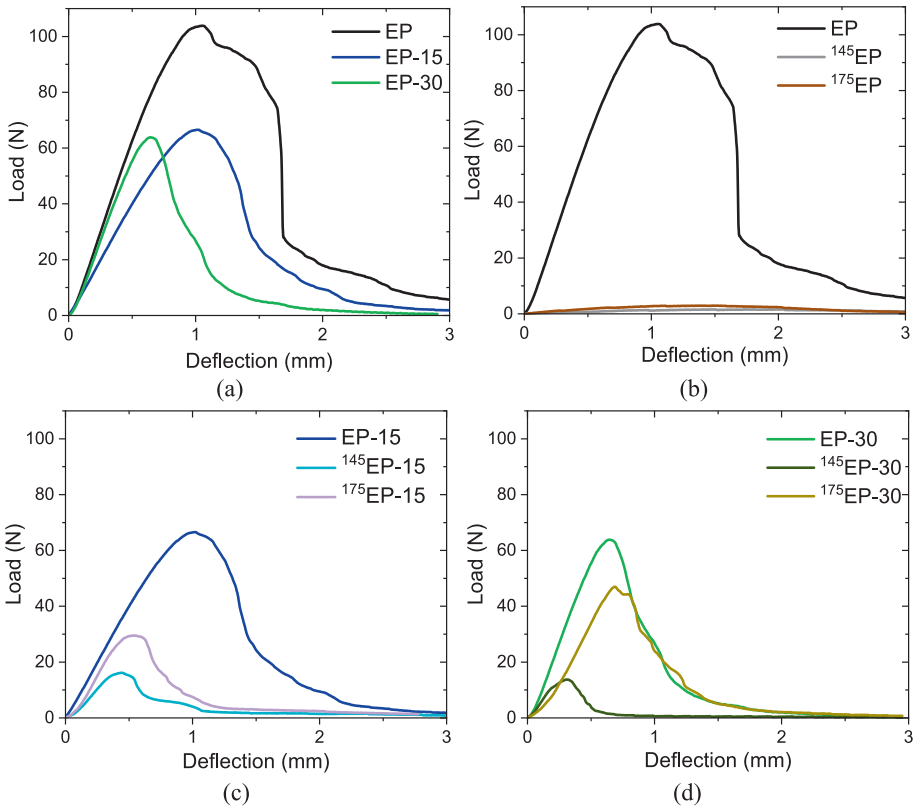

Fig. 7. Representative load–deflection curves from quasi-static flexural tests on the tested SENB specimens. (a) Virgin samples and (b) EP, (c) EP-15, (d) EP-30 samples healed at 145 °C and 175 °C.

Table 5
Results of fracture toughness tests of the virgin and healed EP/COC blends, with the relative healing efficiency values.

Samples	K_{IC} (MPa/$\sqrt{m}$)	$K_{IC,H}$ (MPa/$\sqrt{m}$)	$HE_{K_{IC}}$ (%)	G_{IC} (kJ/m^2)	$G_{IC,H}$ (kJ/m^2)	$HE_{G_{IC}}$ (%)
EP	1.40 ± 0.07	–	–	1.30 ± 0.17	–	–
EP-15	0.96 ± 0.09	–	–	0.84 ± 0.04	–	–
EP-30	1.04 ± 0.08	–	–	1.00 ± 0.04	–	–
^{145} EP	–	0.01 ± 0.01	0.7 ± 0.2	–	0.01 ± 0.01	0.8 ± 0.3
^{145} EP-15	–	0.19 ± 0.06	19.8 ± 6.5	–	0.12 ± 0.04	14.3 ± 4.8
^{145} EP-30	–	0.24 ± 0.05	23.1 ± 5.1	–	0.15 ± 0.06	15.0 ± 6.0
^{175} EP	–	0.03 ± 0.01	2.1 ± 0.6	–	0.01 ± 0.01	0.8 ± 0.2
^{175} EP-15	–	0.50 ± 0.11	52.1 ± 12.4	–	0.20 ± 0.01	23.8 ± 1.6
^{175} EP-30	–	0.84 ± 0.10	80.8 ± 11.4	–	0.55 ± 0.08	55.0 ± 8.3

3.2. Characterization of the bonded joints

3.2.1. Lap shear behaviour and evaluation of the self-healing efficiency

Fig. 9(a-d) shows the load–displacement curves from the lap-shear tests on the prepared joints (both virgin and repaired sample are reported), while Table 6 summarizes the main results.

As can be observed from the curves in Fig. 9a, all joints exhibit a brittle fracture characterized by a sharp decrease in load after the maximum value is reached. The j_EP shows the highest load-bearing capacity and the maximum shear strength (16.2 MP). However, the presence of COC in the adhesive generally reduces the strength of the joint (i.e., 11.6 MPa for j_EP-15 and 14.9 MPa for j_EP-30), attributable to the partial incompatibility between the EP and COC phases. This can result in a premature failure of the joint. However, in the literature [36] and in the fracture toughness tests (Section 3.1.5) it has been observed that debonding is not always disadvantageous, since it involves the local plasticization of the matrix during the debonding process itself. This phenomenon is more intense as the COC content increases and it may explain the recovery of strength in j_EP-30 compared to j_EP-15. Overall, the results suggest that the joints still exhibit shear performance for structural applications, consistently with previous studies [33,34,41].

The load–displacement curves after thermal healing are shown in Fig. 9(b-d). The j_EP shows no lap shear strength recovery, confirming the absence of any intrinsic self-healing capability. By contrast, the EP/COC joints exhibit significant recovery in strength, confirming the activation of the thermoplastic phase upon thermal mending, thanks to the improved interdiffusivity of the COC phase in the matrix above COC's T_g. The ^{175}j_EP-15 sample recovers approximately 21 % of its original strength, while the ^{175}j_EP-30 sample exhibits the greatest recovery, with a τ_{max} of 6.4 MPa and a self-healing efficiency of about 43 %. This higher efficiency value is attributed to the larger availability of the thermoplastic self-healing agent in the EP-30 adhesive. The OM micrographs of the fracture surface of the healed joints further support

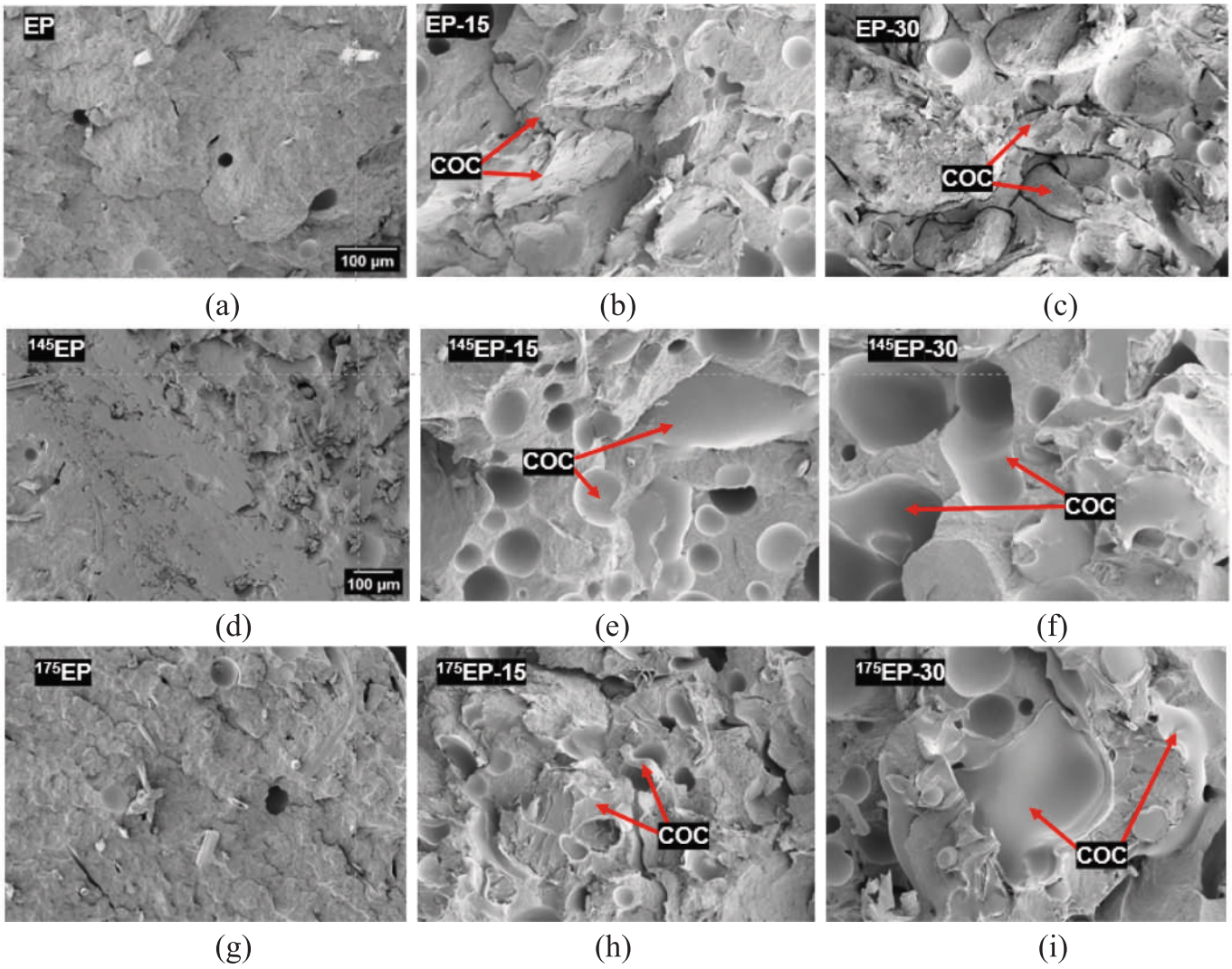

Fig. 8. FESEM micrographs of the fracture surface of the virgin SENB specimens of (a) EP, (b) EP-15 and (c) EP-30. Corresponding micrographs of the SENB specimens healed at (d-f) 145 °C and (g-i) 175 °C.

these findings (Fig. 10).

After healing, the j_EP joint shows a typical adhesive failure, with fracture occurring entirely at the interface between the adhesive and the adherend. By contrast, a progressive transition through thin-layer cohesive failure is observed as the COC content increses meaning that the fracture propagated within the adhesive layer rather than along the interface. This change in failure mode is more evident in case of 30 %wt of COC addition since the larger thermoplastic phase provides more material that softens and flows when heated. Therefore, the molten COC fills the existing cracks and spreads along the adhesive/adherend interface, thereby strengthening the bond between the two. This transition from adhesive to cohesive failure can promote a more effective shear strength recovery. Overall, the lap-shear results confirm that the healing efficiency of the EP/COC joints increases with COC content, which is consistent with the fracture toughness trends observed in the adhesives.

4. Conclusions

In this work, EP/COC blends were investigated as a new type of self-healable adhesives. The work combined the formulation and characterization of the blends, with the fabrication and mechanical testing of bonded FRP joints. Rheological analysis revealed that the incorporation of COC increased the storage modulus, the loss modulus, and the complex viscosity of the blends, since COC limited the macromolecular mobility of the liquid epoxy, rendering the processability of the adhesive more difficult. FTIR spectroscopy and FESEM analysis demonstrated the generation of an immiscible blend with a two-phase morphology, with COC homogeneously dispersed as discrete domains within the epoxy matrix. Thermal analyses highlighted that the system achieved complete curing as well as a good thermal stability. Tensile tests indicated a slight increase in elastic modulus with the addition of COC, but a reduction in tensile strength and elongation at break attributed to poor EP/COC interfacial adhesion. Fracture toughness tests on SENB samples showed a decrease of approximately 26 % and 23 % in K_{IC} and G_{IC}, respectively, for the EP-30 blend compared to neat epoxy, yet the material retained sufficient toughness for structural use. The introduction of the COC phase played a crucial role in enabling the thermal healing, particularly at higher repair temperature (i.e. 175 °C). The EP-30 blend achieved healing efficiencies of approximately 81 % in K_{IC} and 55 % in G_{IC} at 175 °C. FESEM micrographs confirmed that the healing mechanism involved the thermal softening and flow of the COC phase into the damaged areas. In bonded joints, the lap shear tests showed a modest reduction of 8 % in the joint strength with the addition of 30 wt% of COC. After thermal mending at 175 °C, the j_EP-15 sample recovered approximately 21 % of its original lap shear strength, whereas the j_EP-30 sample achieved a strength recovery of 43 %. The transition from adhesive to thin layer-cohesive failure observed in the healed EP-30

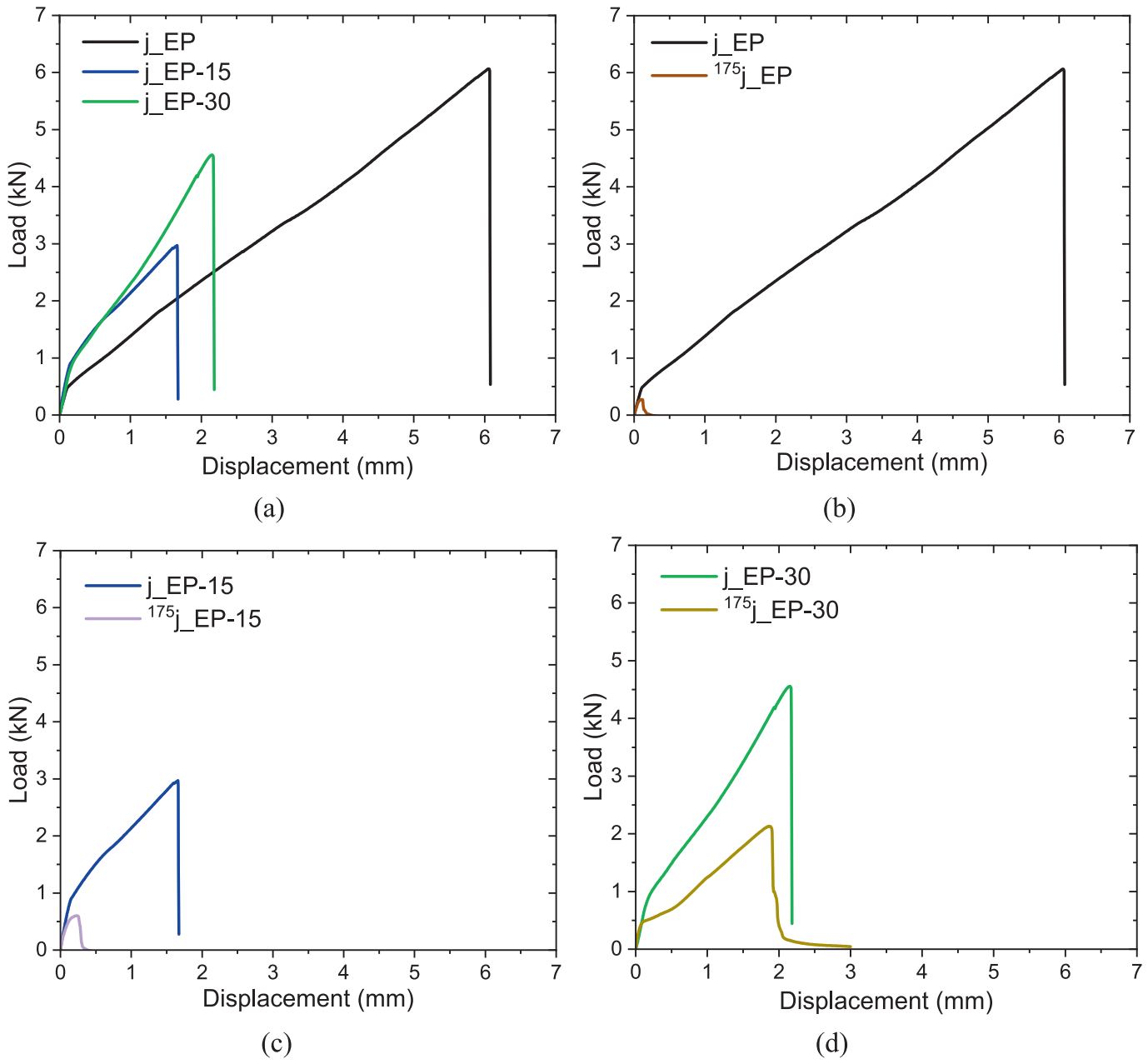

Fig. 9. Representative load–displacement curves from lap shear tests on (a) the virgin joints, and on the joints healed at at 175 °C of (b) j_EP, (c) j_EP-15 and (d) j_EP-30 samples.

Table 6
Results from lap shear tests on the tested joints.

Samples	τ_{max} (MPa)	$\tau_{max,H}$ (MPa)	HE_r(%)
j_EP	16.2 ± 0.3	–	–
j_EP-15	11.6 ± 1.1	–	–
j_EP-30	14.9 ± 1.9	–	–
^{175} j_EP	–	0.2 ± 0.1	1.2 ± 0.2
^{175} j_EP-15	–	2.4 ± 0.5	20.6 ± 4.8
^{175} j_EP-30	–	6.4 ± 1.3	42.8 ± 10.2

joints strongly contributed to promote a more effective shear strength recovery. Overall, the results demonstrated that EP/COC blends combined the structural stiffness of epoxy with the thermal mending capability of COC. In particular, EP/COC blend containing 30 wt% of COC could be a promising self-healing adhesive for use in composite structures, such as wind turbine blades, where the autonomous repair and an extended service life are essential to reduce the maintenance costs and to improve the reliability in harsh conditions. This optimal formulation will be selected for further investigations, including fatigue testing of bonded joints and cyclic self-healing experiments over multiple damage–healing cycles, in order to assess long-term durability and repeatability under service-like conditions.

CRediT authorship contribution statement

Nicolò Truschelli: Writing – review & editing, Investigation, Formal analysis, Data curation. **Laura Simonini:** Writing – original draft, Visualization, Validation, Methodology, Investigation, Conceptualization. **Antonios Tempelis:** Writing – review & editing, Visualization. **Leon Mishnaevsky Jr.:** Writing – review & editing, Visualization. **Alessandro Pegoretti:** Writing – review & editing, Validation,

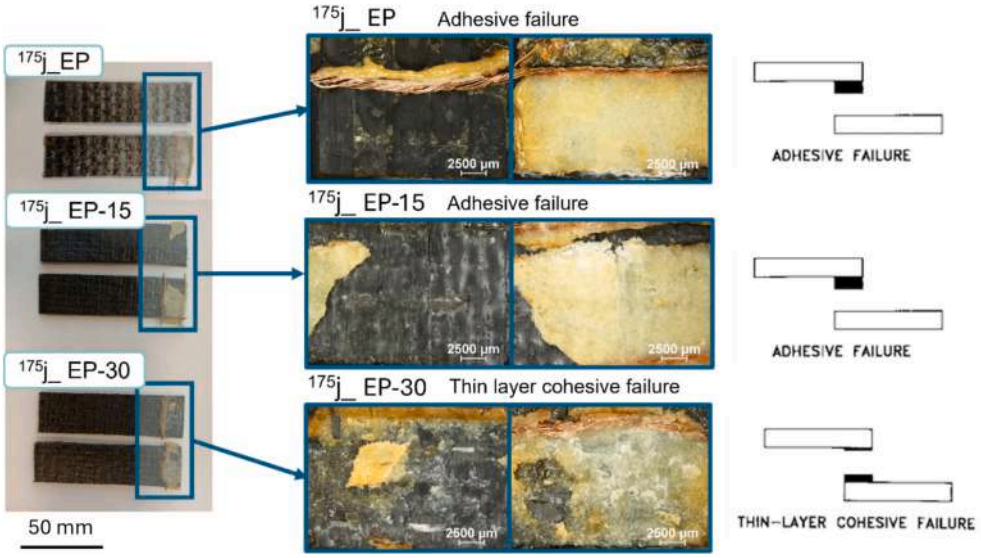

Fig. 10. OM micrographs of the healed joint area after lap shear tests. Adhesive failure is observed in ^{175}j_EP and ^{175} j_EP-15 samples, while thin-layer cohesive failure is observed in ^{175} j_EP-30 sample. The failure mechanism classification is taken from ASTM D5573 standard.

Supervision, Methodology, Conceptualization. **Andrea Dorigato:** Writing – review & editing, Validation, Supervision, Methodology, Conceptualization.

Declaration of competing interest

The authors declare that they have no known competing financial interests or personal relationships that could have appeared to influence the work reported in this paper.

Acknowledgement

A.T. and L.M. acknowledge the financial support of the Velux Foundation via the project PREMISE "Preventing MIcroplastics pollution in SEa water from offshore wind" (https://premise.dtu.dk/), and of the European Commission via Horizon project "Blades2Build: Recycle, repurpose and reuse end-of-life wind blades composites: A coupled pre- and co- processing demonstration plant", grant agreement 101096437.

Appendix A. Supplementary data

Supplementary data to this article can be found online at https://doi.org/10.1016/j.compositesa.2026.109732.

Data availability

Data will be made available on request.

References

[1] GWEC. Wind industry installs record capacity in 2024 despite policy instability, **2025**. Available online: https://www.gwec.net/gwec-news/wind-industry-installs-record-capacity-in-2024-despite-policy-instability (accessed on 17th October 2025).
[2] Barooni M, Ashuri T, Velioglu Sogut D, Wood S, Ghaderpour Taleghani S. Floating offshore wind turbines: current status and future prospects. Energies 2022;16:2–30.
[3] Hong S, McMorland J, Zhang H, Collu M, Halse KH. Floating offshore wind farm installation, challenges and opportunities: a comprehensive survey. Ocean Eng 2024;304:117793–807.
[4] Cao Y, Meng Y, Zhang Z, Yang Q, Li Y, Liu C, et al. Life cycle environmental analysis of offshore wind power: a case study of the large-scale offshore wind farm in China. Renew Sustain Energy Rev 2024;196:114351–67.
[5] Firoozi A, Hejazi F. Innovations in wind turbine blade engineering: exploring materials, sustainability, and market dynamics. Sustainability 2024;16:8564–99.
[6] Reddy SS, Suresh R, Shivakumar BP. Use of composite materials and hybrid composites in wind turbine blades. Mater Today 2021;46:2827–30.
[7] Bošnjaković M, Katinić M, Santa R, Marić D. Wind turbine technology trends. Appl Sci 2022;12:8653–70.
[8] Olabi AG, Wilberforce T, Elsaid K, Sayed ET, Salameh T, Abdelkareem MA, et al. A review on failure modes of wind turbine components. Energies 2021;14:5241–85.
[9] Li H, Teixeira AP, Guedes Soares C. An improved failure mode and effect analysis of floating offshore wind turbines. J Marine Sci Eng 2022;10:1616–31.
[10] Li H, Diaz H, Soares CG. A developed failure mode and effect analysis for floating offshore wind turbine support structures. Renew Energy 2021;164:133–45.
[11] Lopez JC, Kolios A. Risk-based maintenance strategy selection for wind turbine composite blades. Energy Rep 2022;8:5541–61.
[12] Mishnaevsky Jr L. Sustainable end-of-life management of wind turbine blades: Overview of current and coming solutions. Materials 2021;14:1124–49.
[13] Hu Z, Zhang D, Lu F, Yuan W, Xu X, Zhang Q, et al. Multistimuli-Responsive intrinsic self-healing epoxy resin constructed by host–guest interactions. Macromolecules 2018;51:5294–303.
[14] Guimard NK, Oehlenschlaeger KK, Zhou J, Hilf S, Schmidt FG, Barner-Kowollik C. Current trends in the field of self-healing materials. Macromol Chem Phys 2012;213:131–43.
[15] Simonini L, Mahmood H, Dorigato A, Pegoretti A. Evaluation of self-healing capability of a polycaprolactone interphase in epoxy/glass composites. Compos A Appl Sci Manuf 2023;169:107539–48.
[16] Simonini L, Rigotti D, Pidapa J, Pegoretti A. Poly (butylene adipate-co-terephthalate) as a new healing agent for epoxy/basalt composites. Compos A Appl Sci Manuf 2025;196:109010–9.
[17] Simonini L, Kakkonen M, Dsouza R, Kanerva M, Mahmood H, Dorigato A, et al. Tailoring the interfacial properties of glass fiber-epoxy microcomposites through the development of a self-healing poly (ε-caprolactone) coating. Compos Sci Technol 2025;261:110991–1007.
[18] Sun Y, Simonini L, Xing C, Mishnaevsky Jr L. Self-healing interfaces in fiber reinforced polymers: Computational modeling. Compos Sci Technol 2025;270:111269–82.
[19] Simonini L, Canale R, Mahmood H, Dorigato A, Pegoretti A. Multifunctional epoxy/carbon composites with a fully reparable interface. Polym Compos 2024;45:2558–68.
[20] Jones AR, Blaiszik BJ, White SR, Sottos NR. Full recovery of fiber/matrix interfacial bond strength using a microencapsulated solvent-based healing system. Compos Sci Technol 2013;79:1–7.
[21] Hia IL, Chan E-S, Chai S-P, Pasbakhsh P. A novel repeated self-healing epoxy composite with alginate multicore microcapsules. J Mater Chem A 2018;6:8470–8.
[22] Wang Y, Li Y, Zhang Z, Zhao H, Zhang Y. Repair performance of self-healing microcapsule/epoxy resin insulating composite to physical damage. Appl Sci 2019;9.
[23] Zhang W, Duchet J, Gerard JF. Self-healable interfaces based on thermo-reversible Diels–Alder reactions in carbon fiber reinforced composites. J Colloid Interface Sci 2014;430:61–8.
[24] Strachota B, Hodan J, Dybal J, Matějka L. Self-Healing epoxy and reversible diels-alder based interpenetrating networks. Macromol Mater Eng 2021;306:2000474–88.
[25] Kosarli M, Bekas DG, Tsirka K, Baltzis D, Vaimakis-Tsogkas DT, Orfanidis S, et al. Microcapsule-based self-healing materials: healing efficiency and toughness reduction vs. capsule size. Compos B Eng 2019;171:78–86.
[26] Malekkhouyan R, Neisiany RE, Khorasani SN, Das O, Berto F, Ramakrishna S. The influence of size and healing content on the performance of extrinsic self-healing coatings. J Appl Polym Sci 2021;138:49964–78.

[27] Perin D, Mahmood H, Rigotti D, Dorigato A, Pegoretti A. Novel epoxy/cyclic olefin copolymer/carbon structural composites with electro-activated self-healing properties. Polym Compos 2023;44:5173–87.
[28] Zovi RC, Mahmood H, Dorigato A, Fredi G, Pegoretti A. Cyclic olefin copolymer interleaves for thermally mendable carbon/epoxy laminates. Molecules 2020;25:5347.
[29] Pei X, Li Y, Zhao S, He X. Viscoelasticity, tensile properties, and microstructure development in cyclic olefin copolymer/polyolefin elastomer blends. Macromol Chem Phys 2022;223:2200018–38.
[30] Wan X, Demir B, An M, Walsh TR, Yang N. Thermal conductivities and mechanical properties of epoxy resin as a function of the degree of cross-linking. Int J Heat Mass Transf 2021;180:121821–41.
[31] Dorigato A, Mahmood H, Pegoretti A. Optimization of the thermal mending process in epoxy/cyclic olefin copolymer blends. J Appl Polym Sci 2021;138:49937–52.
[32] Mahmood H, Dorigato A, Pegoretti A. Thermal mending in novel epoxy/cyclic olefin copolymer blends. Express Polym Lett 2020;14:368–83.
[33] Dorigato A, Pegoretti A, Bondioli F, Messori M. Improving epoxy adhesives with zirconia nanoparticles. Compos Interfaces 2010;17:873–92.
[34] Dorigato A, Pegoretti A. The role of alumina nanoparticles in epoxy adhesives. J Nanopart Res 2011;13:2429–41.
[35] Da Silva LF, Rodrigues TNSS, Figueiredo MAV, De Moura MFSF, Chousal JAG. Effect of adhesive type and thickness on the lap shear strength. J Adhes 2006;82:1091–115.
[36] Perin D, Dorigato A, Pegoretti A. Thermoplastic self-healing polymer blends for structural composites: Development of polyamide 6 and cyclic olefinic copolymer blends. J Appl Polym Sci 2023;140:53751–68.
[37] Ackermann AC, Carosella S, Rettenmayr M, Fox BL, Middendorf P. Rheology, dispersion, and cure kinetics of epoxy filled with amine-and non-functionalized reduced graphene oxide for composite manufacturing. J Appl Polym Sci 2022;139:51664–79.
[38] Meure S, Wu DY, Furman SA. FTIR study of bonding between a thermoplastic healing agent and a mendable epoxy resin. Vib Spectrosc 2010;52:10–5.
[39] Li L, Wu R, Guang S, Su X, Xu H. The investigation of the hydrogen bond saturation effect during the dipole–dipole induced azobenzene supramolecular self-assembly. Phys Chem Chem Phys 2013;15:20753–63.
[40] Abbasi E, Jannesari A. Thermogravimetric analysis of a new series of trimellitimide-based epoxy-imide resins. Thermochim Acta 2024;38:179793–806.
[41] Dorigato A, Pegoretti A. Development and thermo-mechanical behavior of nanocomposite epoxy adhesives. Polym Adv Technol 2012;23:660–8.